Journal of Power Sources 283 (2015) 423–428

Contents lists available at ScienceDirect

Journal of Power Sources

journal homepage: www.elsevier.com/locate/jpowsour

Short communication

Unconventional irreversible structural changes in a high-voltage Li–Mn-rich oxide for lithium-ion battery cathodes

Debasish Mohanty [a, *], Athena S. Sefat [b], E. Andrew Payzant [c], Jianlin Li [a], David L. Wood III [a], Claus Daniel [a]

[a] Energy and Transportation Science Division, Oak Ridge National Laboratory, Oak Ridge, TN 37831, USA
[b] Materials Science and Technology Division, Oak Ridge National Laboratory, Oak Ridge, TN 37831, USA
[c] Chemical and Engineering Materials Division, Oak Ridge National Laboratory, Oak Ridge, TN 37831, USA

HIGHLIGHTS

- Irreversible phase transformation in a high-voltage Li–Mn-rich oxide is demonstrated.
- Magnetization technique is employed to ascertain the major spinel phase.
- A spin-glass type transition is observed, indicating a dominant $LiMn_2O_4$ type spinel.
- Irreversible phase transformation leads to voltage and/or capacity fading.

GRAPHICAL ABSTRACT

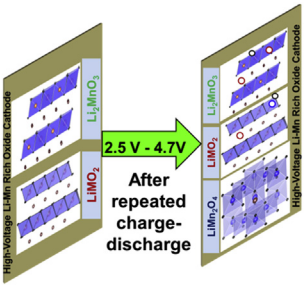

ARTICLE INFO

Article history:
Received 23 December 2014
Received in revised form
14 January 2015
Accepted 16 February 2015
Available online 19 February 2015

Keywords:
Lithium rich
Structural transformation
Spinel
High-energy-density lithium-ion batteries
Magnetic frustration

ABSTRACT

Making *all*-electric vehicles (EVs) commonplace in transportation applications will require affordable high-power and high-energy-density lithium-ion batteries (LIBs). The quest for suitable cathode materials to meet this end has currently plateaued with the discovery of high-voltage (≥4.7 V vs. Li^+), high capacity (~250 mAh/g) lithium–manganese-rich (LMR) layered composite oxides. Despite the promise of LMR oxides in high-energy-density LIBs, an irreversible structural change has been identified in this work that is governed by the formation of a 'permanent' spin-glass type magnetically frustrated phase indicating a dominant AB_2O_4 (A = Li, B = Mn) type spinel after a short-term lithium deintercalation (charging) and intercalation (discharging) process. Furthermore, reduction of transition metal (Mn) ions from the 4+ state (pristine LMR) to 3+ (cycled LMR), which alters the intercalation redox chemistry and suggests the presence of 'unfilled' lithium vacancies and/or oxygen vacancies in the lattice after cycling, has presented a major stumbling block. These situations result in both loss of capacity and fading of the voltage profile, and these combined effects significantly reduce the high energy density over even short-term cycling.

1. Introduction

Today's energy storage devices in EVs require advanced high power and high-energy-density lithium-ion batteries (LIBs) [1–3]. LIB energy density is directly proportional to specific capacity and average operating voltage (energy density = specific

* Corresponding author. Energy and Transportation Science Division Oak Ridge National Laboratory, One Bethel Valley Road, Oak Ridge, TN 37831, USA.
E-mail address: mohantyd@ornl.gov (D. Mohanty).

http://dx.doi.org/10.1016/j.jpowsour.2015.02.087
0378-7753/

capacity × average operating voltage). Lithium-containing layered metal oxide (ex: $LiMO_2$; M = Ni, Mn, Co or NMC) materials are the state-of-the-art commercial cathode materials in current LIBs. These layered oxides have tremendous capabilities for facile lithium (de)intercalation reactions [4,5]. The charge and discharge processes in a LIB involve deintercalation and intercalation of lithium ions from and to the cathode structure, respectively [6]. Therefore, maintaining the original oxide structure through the repeated charge–discharge cycles is a vital to long-term performance. Current state-of-the-art cathode nickel–manganese–cobalt (NMC) oxides (such as $LiNi_{1/3}Mn_{1/3}Co_{1/3}O_2$) maintain the original host structure without undergoing alteration after several charge–discharge cycles. Unfortunately, these oxides are limited in energy density because of lower operating voltages (~4.2 V) and lower practical capacity (~160 mAh/g) [7]. However, adding an excess of lithium in place of transition metals (M) in the NMC oxide maintains the layered structure and dramatically increases the capacity and operating voltage [8–12]. For instance, with 20% excess lithium and a stoichiometrically proportionate increase in Mn to $Li_{1.2}Ni_{0.15}Mn_{0.55}Co_{0.1}O_2$ (in this study), a remarkable reversible capacity of 250 mAh/g can be achieved at high operating voltage (~4.7 V) [13,14]. These lithium–manganese-rich (LMR) layered oxides are promising cathode candidates for high voltage, high capacity (high-energy-density) LIBs for EV applications, but they are hampered by a layered-to-spinel structural degradation during cycling [15–19].

Here we present that despite these excellent beginning-of-life properties, LMR oxides undergo an unconventional 'irreversible' structural change after minimal numbers of charge–discharge cycles (25 in this study) that severely degrade performance by blocking the ion transport pathways in the oxide lattice. In this study, our inquisition is focused on answering these important questions; i) Is this structural change irreversible? ii) How do these irreversible structural and electronic changes occur? iii) What is the dominant 'spinel' phase formed after structural changes? iv) What is the impact of these irreversible structural changes on the lithium-ion transport phenomena? In order to obtain fundamental insight into these irreversible structural changes, we executed temperature-dependent magnetic susceptibility combined with selected area electron diffraction (SAED) on LMR oxides harvested from *full LIB pouch cells* at different states of charge (SOCs) during early (second) cycle and after short-term (25) cycles (see S1 in ESI). The motivation behind employing the magnetic susceptibility technique [20] was to take advantage of its sensitivity in detecting subtle structural changes, as well as the electronic states of transition metal (M) ions, as compared to other conventional techniques such as diffraction and its ability to distinguish the crystal structure of different types of spinel compound such as tetragonal spinel and cubic spinel.

2. Experimental

The LMR oxide powder used in this study was synthesized by TODA America, Inc., (alternate name:HE5050) and the composition, *ex and in situ* XRD, particle morphology, selected area electron diffraction (SAED), high-resolution transmission electron microscopy (HR-TEM) images, and electrochemical performance data can be found in earlier report [16]. LMR electrode and pouch cell fabrication was reported previously [21]. All full cells (with ConocoPhillips A12 graphite anodes) underwent formation cycling following a procedure reported elsewhere [13] and were cycled between 2.5 and 4.7 V for 26 cycles at a rate of 20 mA/g. Cathode samples were collected at different SOCs (3.2, 3.5, 4.1, and 4.5 V) during the second and 26th charge–discharge cycles. All pouch cells were disassembled in an argon-containing glove box, washed with dimethyl carbonate (DMC), and dried for several hours in the glove box. Cycled LMR oxide powder materials were removed from the Al current collectors after being dried for selected area electron diffraction (SAED) experiments. For temperature dependent magnetic susceptibility experiments, half-inch diameter specimens were punched from the cycled LMR oxide electrodes. These specimens contained LMR active oxides, PVDF binder, carbon black, and Al foil. A Quantum Design Magnetic Property Measurement System was used to measure the DC magnetization of the specimens. Each sample was first cooled to 5 K in zero field (zero-field cooling mode, represented as ZFC). Then a field of 100 Oe was applied, and data were collected from $T = 5$ K–300 K. The samples were also cooled in the applied field from 300 K down to 5 K while magnetization was measured (field cooling, represented as FC). The experimental effective magnetic moment was obtained from a linear fit of the plot of inverse molar magnetic susceptibility vs. temperature between 150 and 300 K using the Curie–Weiss equation $\chi_m = C_m(T - \theta)$, where χ_m is the molar magnetic susceptibility, C_m is the Curie constant, and θ is the Curie–Weiss temperature. For SAED experiments, the harvested cycled powder was dispersed in ethanol and few drops of the solution were added to a holey Cu grid. A Hitachi HF3300 TEM at 300 kV was used to collect SAED patterns.

3. Results and discussion

The structure of $Li_{1.2}Ni_{0.15}Mn_{0.55}Co_{0.1}O_2$ (LMR here onward) oxide is a composite of layered $xLiMO_2$ (Phase I) and layered $(1 - x)$ Li_2MnO_3 (Phase II)composition (x = 0.5 in this study). $LiMO_2$ attains a typical α-$NaFeO_2$ type structure having a trigonal lattice, where the transition metal (M; Co, Mn, Ni) ions are freely occupied in octahedral metal sites, so magnetic moments are non-interacting and are not aligned in a regular pattern (randomly oriented) such that Curie–Weiss (CW) paramagnetic behavior (Fig. 1 and Fig. 2e) is expected. The excess lithium ions present in the LMR structure occupy the M layer, filling all the octahedral sites of cubic close-packed (*ccp*) oxygen arrays. The presence of lithium ions in the M

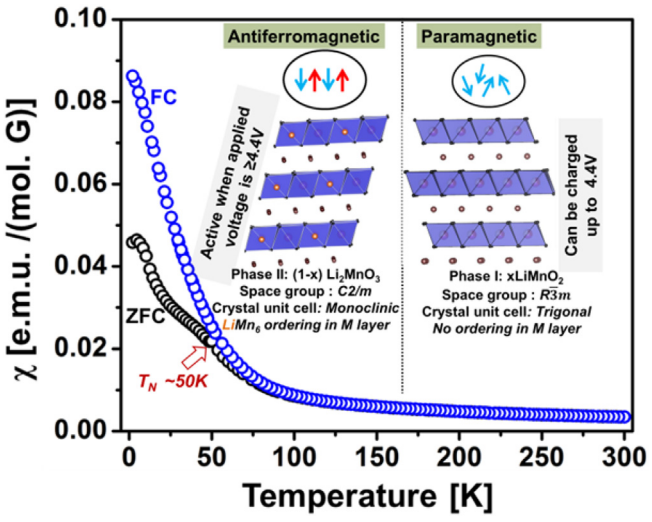

Fig. 1. Temperature dependent magnetic susceptibility data from pristine LMR oxide at field cooling (FC) and zero field cooling (ZFC) modes. At higher temperature paramagnetic nature is observed indicating presence of trigonal $LiMO_2$ lattice (Phase I) and at low temperature antiferromagnetic transition occurs at T_N ~ 50 K indicating a second monoclinic Li_2MnO_3 phase (Phase II) where lithium is present in the M layer ($LiMn_6$ ordering) in pristine LMR oxide. Lithium intercalation from Phase II occurs beyond 4.4 V charging. Adapted (modified) with permission from *Chem. Mater.*, 2013, 25 (20), pp 4064–4070. Copyright 2013 American Chemical Society [23].

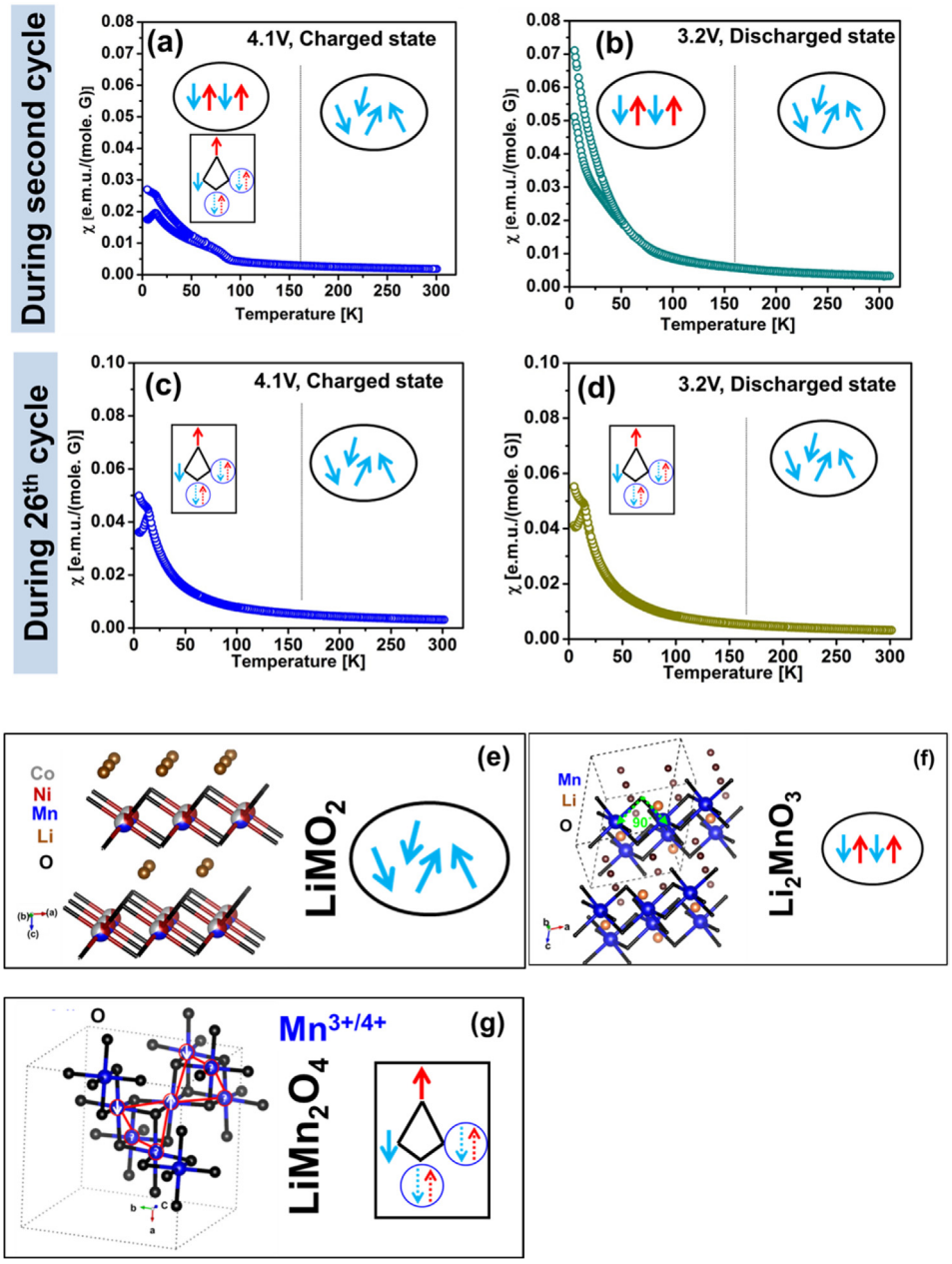

Fig. 2. Magnetic susceptibility vs. temperature data for the LMR oxides at 4.1 V charged states (a: during second cycle, c: during 26th cycles) and 3.2 V discharged states (b: during second cycle, d: during 26th cycle). Different types of magnetic interactions in trigonal $LiMO_2$ (e), monoclinic Li_2MnO_3 (f), and cubic spinel $LiMn_2O_4$ (g). Trigonal $LiMO_2$ has mixed M (Co, Mn, Ni) occupancies in the M layer that creates the paramagnetic interactions (e). In monoclinic Li_2MnO_3, 90° interaction between $Mn^{4+}(d^3)$ ions via O anion creates strong antiferromagnetic interaction (f). Cubic spinel with composition $LiMn_2O_4$ with dual Mn oxidation states create magnetic frustration in Mn_2O_4 units.

layer generates the cation ordering of Li^+ with the Mn^{4+} ($LiMn_6$) ions that leads to formation of a second Li_2MnO_3 component with monoclinic lattice. In an Li_2MnO_3 component, octahedra $Mn^{4+}(d^3)$ share edges, and a 90° $Mn^{4+}(d^3)$-O-$Mn^{4+}(d^3)$ magnetic exchange interaction (Fig. 2f) is possible, which is strongly antiferromagnetic (AFM) [22]. Temperature dependent magnetic susceptibility on the pristine LMR oxide is reported elsewhere [23]. Briefly, the magnetization data shows similar paths of field cooling (FC, blue circle (in web version) in Fig. 1) and zero field cooling (ZFC, black circles in Fig. 1) at the higher temperature region ($T \geq 150$ K), and confirms the presence of M ions with randomly oriented magnetic moments (of M ions) from the layered $LiMO_2$ component (phase I) having trigonal lattice. At $T \sim 50$ K (denoted as the Neel temperature; T_N), bifurcation of FC and ZFC occurs showing a AFM behavior that strongly suggests the presence of the Li_2MnO_3 component (Phase II) where Mn ions are antiferromagnetically coupled to each other via oxygen anions. The oxidation states of M ions calculated from the Curie–Weiss fit applied to the inverse susceptibility data at $150 \geq T \leq 300$ K (see S2 in ESI) gives an effective magnetic moment value of 3.06 μ_B that is in agreement with magnetic model having Ni in 2+, Mn in 4+ and Co in 3+ states (theoretical magnetic moment is 3.07 μ_B). In this class of LMR oxides, Ni^{2+} and Co^{3+} are the electrochemically active ions that participate in the electrochemical redox reactions, and Mn plays a significant role towards maintaining the structural stability [1]. In the next section, we will show that there could be structural irreversibility in initial cycles

(second cycle); however, significant irreversible structural changes occur after minimal charge–discharge cycles (25 cycles).

Magnetic susceptibility data from the cycled LMR oxides at different SOCs in the second and 26th cycles (see S3 and S4 in ESI and Fig. 2a-d) provided evidence of Curie–Weiss type paramagnetic behavior at the higher temperature region ($T \geq 150$ K) which showed the presence of the trigonal $LiMO_2$ component in the structure. As mentioned above, the bifurcation of the FC and ZFC curves in the lower temperature region ($T \leq 60$ K) is a signature of $LiMn_6$ ordering in Li_2MnO_3 component. Note that the magnetic transition at $T_N \sim 50$ K is observed (insets of S2) in all oxides at different SOCs in the second cycle. To quantify the cation ordering that is directly correlated to the strength of the bifurcation, we calculated the area between the FC and ZFC curves (see S5 and S6 in ESI) and compared it with the pristine LMR oxide. It is evident that during the second cycle, the bifurcation of the FC and ZFC curves gradually decreased during charging and recovered at the discharge state of 3.2 V with a reduced strength as compared to the pristine LMR oxide (compare Fig. 1 and Fig. 2b). The decrease in bifurcation strength is an indication of a decrease in the $LiMn_6$-like region (i.e., a decrease in the Li_2MnO_3 component) in this class of LMR oxides. Interestingly, the strength of bifurcation was substantially reduced (or not observed) in the LMR oxides in the 26th cycle (Fig. S6 in ESI and Fig. 2c, d) indicating the presence of minimal $LiMn_6$ –like regions in the LMR oxides after 25 cycles. The results also revealed a different type of magnetic feature (cusp-like behavior of FC and ZFC curves) in the LMR oxide during second-cycle charging (4.1 V, 4.5 V) and discharging (4.1 V, 3.5 V), but this feature was not observed at the 3.2 V discharged state (Fig. S3). Therefore, after the second cycle, significant modification in the LMR oxide structure was not evidenced, however reduced cationic ordering in Li_2MnO_3 component is observed. Interestingly, during 26th cycle the irreversible cusp-like behaviors was observed below ~11 K (Fig. 2c and d and Fig. S4 in ESI) for all harvested oxides regardless of SOC values. This feature is an indication of a spin-glass (SG) like feature [24] in the lattice after the second cycle that becomes permanent after 25 cycles, which is not expected in the case of structures with only trigonal or monoclinic lattices. The SG behavior may be due to the i) presence of mixture of ferromagnetic and antiferromagnetic interactions in LMR oxide that becomes more prominent when the strength of cationic ordering is reduced, and/or ii) presence of a charge-frustrated lattice exclusively in the $LiMn_2O_4$ unit cell. However, the reduction of Mn from 4+ to 3+ (see the section below) indicate that $LiMn_2O_4$ spinel may have been formed in the lattice that shows the magnetic frustration. In addition to this, in case of $LiMn_2O_4$ cubic spinel [24,25], magnetic moments from two Mn atoms are antiferromagentically aligned, and the moments from other two Mn atoms are either ferromagnetically or antiferromagnetically coupled. The magnetic moments from two magnetic ions, Mn^{3+}, and Mn^{4+} in the $LiMn_2O_4$ lattice occupy in a random manner generating a charge-frustrated lattice showing SG-like behavior (Fig. 2g). It should be noted that the SG-type behavior may also be observed in the case of a $Li_2Mn_2O_4$-like spinel (tetragonal spinel); however, this structure would show a different magnetic feature where a low magnetic moment would be observed for the FC curve [26]. In addition, the prominent cusp-like feature would not be seen in tetragonal $Li_2Mn_2O_4$ spinel, which is due to the difference in the two spinel crystal structures (tetragonal spinel for $Li_2Mn_2O_4$ vs. cubic spinel for $LiMn_2O_4$). Because of the tetragonal distortion in $Li_2Mn_2O_4$, a short-range antiferromagnetic interaction would be observed, and this was not the case for the LMR oxides harvested after 25 cycles. Therefore, the magnetic susceptibility data in this study was able to resolve the nature of dominant 'spinel' phase in the cycled LMR oxides and provides evidence of irreversible structural changes after short-term cycling.

In order to demonstrate the alteration in the redox process, we calculated effective magnetic moments by applying CW fitting to the inverse magnetic susceptibility data between $150K \leq T \leq 300$ K of LMR oxides harvested at different SOCs (Figs. S7 and S8 in ESI). During the second cycle, the effective magnetic moment for the material charged to 4.1 V was calculated as 2.6 μB, which is less than the value obtained for the pristine LMR oxide (3.06 μB). This decrease in magnetic moment is due to oxidation of Ni^{2+} (LS/HS: S = 1) to Ni^{3+} (LS: S = 1/2)/Ni^{4+} (LS: S = 0) during lithium-ion extraction from the LMR host lattice. The magnetic moment slightly increased to 2.67 μB when charged further (to 4.5 V). When discharged back to 4.1 V, though, the effective magnetic moment further increased to 2.78 μB and continued increasing upon further discharging (2.98 μB at 3.5 V) to a final value of 3.01 μB at the 3.2 V. This increase in effective magnetic moment during discharging indicates reduction of Ni^{3+} (LS: S = 1/2)/Ni^{4+} (LS: S = 0) to Ni^{2+} (LS/HS: S = 1) by a charge-compensation reaction due to lithium-ion insertion into the LMR host lattice. After completion of second cycle at 3.2 V, the cycled LMR oxide attained an effective magnetic moment slightly less than that of the pristine LMR oxide. However, during 26th cycle, the effective magnetic moment at the 3.2-V charged state was 2.91 μB. This parameter decreased for the oxide collected at 4.1 V (2.65 μB) and increased slightly (2.71 μB) for the oxide collected at the 4.5 V. During discharging, the effective magnetic moment increased to 2.92 μB at 4.1 V, to 2.94 μB at 3.5 V, and to 3.10 μB at 3.2 V. The decrease in the effective magnetic moment during charging and its increase during discharging may be explained by similar reasons described for the second cycle. However, the effective magnetic moment at the 3.2-V discharged state was larger than the value obtained after completion of second cycle and the pristine LMR oxide. This clearly suggests the presence of Mn^{3+} (d^4 configuration, which has a higher magnetic moment than d^3 configuration in Mn^{4+}) from a $LiMn_2O_4$ -like unit cell in the lattice. The presence of Mn of different oxidation states (3+ and 4+) in the $LiMn_2O_4$ unit cell eventually generates a condition for charge frustration in Mn_2O_4 units. Therefore, a SG-type lattice in LMR oxides indicates the presence of permanent and dominant $LiMn_2O_4$ spinel phase after 25 cycles. The representative SAED patterns from pristine LMR oxides, after the second cycle at the 3.2 V discharged state and after the 26th cycle at the 3.2 V discharged sate (Fig. 3a–c respectively) show a decrease in intensity of cationic ordering peaks (yellow marked arrows) during the second cycle and new spinel type diffraction spots [14] after the 26th cycle (red marked arrow). This result is in accordance with the magnetic susceptibility data presented above, i.e. irreversible structural changes in LMR oxides after a short-term cycling. In the next section, we present an explanation for this irreversible structural change and its effect on LIB performance.

During low-voltage charging (≤4.4 V), lithium ions are extracted from the lithium layer of the LMR oxide structure. Beyond ~4.4 V, lithium-ion diffusion occurs from the M layer of the Li_2MnO_3 component (Phase II), which provides the high-capacity and allows for high-voltage operation. In order to continue delivering high-capacity at high-voltage, these lithium ions must travel back to their respective sites (lithium and M layers) and the Li_2MnO_3 component must be maintained for facilitating this process. However, charging beyond 4.4 V (when the Li_2MnO_3 becomes active) and extracting lithium ions from the M layers destroys the $LiMn_6$-type ordering. As evidenced from the area of FC and ZFC curves during the second cycle, the strength of bifurcation of the FC and ZFC curves decreases at the 3.2 V discharged state after completion of second cycle. After the 26th cycle, bifurcation is significantly reduced confirming that lithium ions are trapped and/or relocated in different crystallographic sites, which creates vacancies in the original lithium

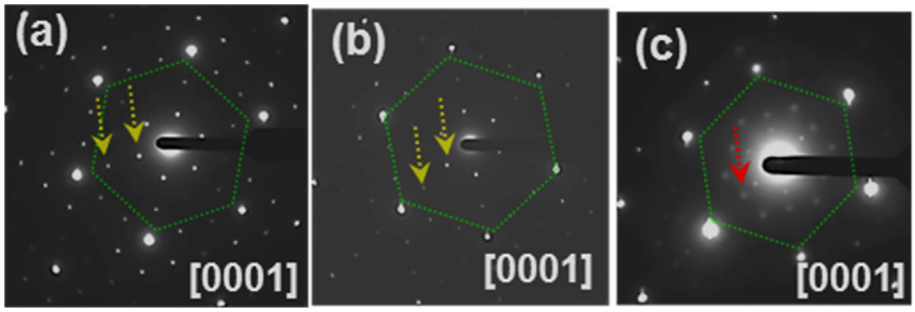

Fig. 3. Selected area electron diffraction (SAED) of pristine (a), after completion of second cycle at 3.2 V discharged state (b), and after completion of 26th cycle at 3.2 V discharged state (c). The bright fundamentals spots (marked as hexagon) are from trigonal $LiMO_2$ unit cell (Phase I). The spots indicating the cationic ordering ($LiMn_6$ like regions in monoclinic) are marked as yellow arrows (Phase II) and the spot from spinel unit cell is marked as red arrow. The cationic ordering peak intensity decreases substantially after 26th cycle and the spinel spot was observed after 26th cycles. (For interpretation of the references to color in this figure legend, the reader is referred to the web version of this article.)

sites (Li_V). Eventually, most of the lithium atoms in the transition metal layers of Li_2MnO_3 component likely do not travel back to their original sites after short-term cycling. Lithium vacancies in the LMR structure and the presence of Mn^{3+} in the lattice further indicate oxygen loss [10,27–30] from the structure for charge compensation, a model similar to previous observations made by other researchers. Once the oxygen vacancies (O_V) are formed, M ions in M layer (M_M) could migrate to the vacant lithium layer via vacant oxygen sites ($M_M \rightarrow O_V \rightarrow Li_V$). This process might be irreversible after second cycle, however prominent irreversibility was observed after repeated charge–discharge cycles (26 in this case) that create stable Mn_2O_4-like units to form $LiMn_2O_4$ spinel. The lithium vacancies and oxygen loss lead to an irreversible phase change in this candidate high-voltage cathode (HVC) and alter the lithium transport phenomena by blocking the diffusion paths in the host lattice. One of the impacts of these irreversible structural changes is capacity fade because of significant available lithium loss during the (de)intercalation process. The decrease in lithium occupancies in the host LMR oxide further alters the SOC at a given capacity causing suppression of the voltage profile. This condition gradually deteriorates the energy and power density of LIBs [21].

4. Conclusions

This work shows direct evidence of unconventional irreversible structural changes in a candidate HVC LMR oxide for high-energy-density LIBs. We implemented the temperature dependent magnetization technique to elucidate these phenomena and demonstrate magnetic susceptibility technique as one of the important materials diagnostic methods to understand the structural changes in 'complex' layered oxides. This technique took advantage of electron spins (magnetic moments) in the deconvolution of a dominant 'spinel' phase after repeated charging and discharging. A spin glass (SG) magnetic frustrated lattice suggested the presence of a charge frustrated Mn_2O_4 unit in the $LiMn_2O_4$ spinel lattice. The results presented here support the hypothesis that the layered LMR material transforms to spinel ($LiMn_2O_4$ as the dominant phase) because of formation of lithium vacancies and oxygen loss and lead to capacity and voltage fading. Despite the remarkable reversible capacity of LMR oxides, suppression of these unacceptable irreversible structural and transition metal electronic state changes leading to voltage fading prevents the materials from utility beyond several hundred charge–discharge cycles.

Acknowledgments

This research at Oak Ridge National Laboratory, managed by UT Battelle, LLC, for the U.S. Department of Energy (DOE) under contract DE-AC05-00OR22725, was sponsored by the DOE Energy Efficiency and Renewable Energy (EERE), Vehicle Technologies Office (VTO), Applied Battery Research (ABR) Program (Program Managers: Peter Faguy and David Howell). Part of this research was supported by the DOE Basic Energy Sciences (BES), Materials Sciences and Engineering Division. A portion of this research was conducted at the Center for Nanophase Materials Sciences, which is a DOE Office of Science User Facility. The LMR oxide was obtained from Argonne National Laboratory, in collaboration with Andrew Jansen and Bryant Polzin. The electrodes and cell fabrication and pouch cell testing were carried out at the DOE Battery Manufacturing R&D Facility at Oak Ridge National Laboratory (BMF), which is supported by VTO's ABR Program. We specially thank Dr. Daniel P. Abraham from Argonne National Laboratory for his invaluable help to design the electrochemical experiments for this study.

Appendix A. Supplementary data

Supplementary data related to this article can be found at http://dx.doi.org/10.1016/j.jpowsour.2015.02.087.

References

[1] M.M. Thackeray, C. Wolverton, E.D. Isaacs, Energy Environ. Sci. 5 (2012) 7854.
[2] S.S. Zhang, Front. Energy Res. 1 (2013) 1.
[3] D.T. Danielson, EV Everywhere Grand-challenge Blue Print, 2013. http://www1.eere.energy.gov/vehiclesandfuels/electric_vehicles/pdfs/eveverywhere_blueprint.pdf. Energy, U. S. D. o., Ed.
[4] M.S. Whittingham, Chem. Rev. 104 (2004) 4271.
[5] M.S. Whittingham, Mater. Res. Bull. 33 (2008) 411.
[6] J.M. Tarascon, M. Armand, Nature 451 (2008) 652.
[7] H. Yu, R. Shikawa, Y.-G. So, N. Shibata, T. Kudo, H. Zhou, Y. Ikuhara, Angew. Chem. 52 (2013) 5969.
[8] M.M. Thackeray, C.S. Johnson, J.T. Vaughey, N. Li, S.A. Hackney, J. Mater. Chem. 15 (2006) 2257.
[9] M.M. Thackeray, S-Ho Kang, C.S. Johnson, J.T. Vaughey, R. Benedek, S.A. Hackney, J. Mater. Chem. 17 (2007) 3112.
[10] N. Yabuuchi, K. Yoshii, S.-T. Myung, I. Nakai, S. Komaba, J. Am. Chem. Soc. 133 (2011) 4404.
[11] Z.H. Lu, D.D. MacNeil, J.R. Dahn, Electrochem. Solid State Lett. 4 (2001) A191.
[12] M. Sathiya, A.M. Abakumov, D. Foix, G. Rousse, K. Ramesha, M. Saubanère, M.L. Doublet, H. Vezin, C.P. Laisa, A.S. Prakash, D. Gonbeau, G. VanTendeloo, J.-M. Tarascon, Nat. Mater. 14 (2015) 230238.
[13] Y. Li, M. Bettge, B. Polzin, Y. Zhu, M. Balasubramanian, D.P. Abraham, J. Electrochem. Soc. 160 (2013) A3006.
[14] D. Mohanty, A.S. Sefat, J. Li, R.A. Meisner, A.J. Rondinone, E.A. Payzant, D.P. Abraham, D.L. Wood III, C. Daniel, Phys. Chem. Chem. Phys. 15 (2013) 19496.
[15] K.G. Gallagher, J.R. Croy, M. Balasubramanian, M. Bettge, D.P. Abraham, A.K. Burrell, M.M. Thackeray, Electrochem. Commun. 33 (2013) 96.
[16] D. Mohanty, S. Kalnaus, R.A. Meisner, K.J. Rhodes, J. Li, E.A. Payzant, D.L. . Wood III, C. Daniel, J. Power Sources 229 (2013) 239–248.
[17] B. Song, Z. Liu, M. On Lai, L. Lu, Phys. Chem. Chem. Phys. 14 (2012) 12875.
[18] M. Gu, I. Belharouak, J. Zheng, H. Wu, J. Xiao, A. Genc, K. Amine,

S. Thevuthasan, D.R. Baer, Ji-G. Zhang, N.D. Browning, J. Liu, C. Wang, ACS Nano 7 (2013) 760–767.
[19] P.K. Nayak, J. Grinblat, M. Levi, B. Markovsky, Doron Aurbach, J. Electrochem. Soc. 161 (2014) A1534–A1547.
[20] N.A. . Chernova, G.M. Nolis, F.O. Omenya, H. Zhou, Z. Lia, M.S. Whittingham, J. Mater. Chem. 21 (2011) 9865.
[21] D. Mohanty, J.L. Li, D.P. Abraham, A. Huq, E.A. Payzant, D.L. Wood III, C. Daniel, Chem. Mater. 26 (2014) 6272.
[22] J.B. Goodenough, Phys. Rev. 117 (1960) 1442.
[23] D. Mohanty, A. Huq, E. Andrew Payzant, A.S. Sefat, J. Li, D.P. Abraham, D.L. Wood III, C. Daniel, Chem. Mater. 25 (2013) 4064–4070.
[24] Y-Il Jang, F.C. Chou, Y-Ming Chiang, Appl. Phys. Lett. 74 (1999) 2504.
[25] A.S. . Wills, N.P. Raju, J.E. Greedan, Chem. Mater. 11 (1999) 1510–1518.
[26] Y-Il Jang, B. Huang, F.C. Chou, D.R. Sadoway, Y-Ming Chiang, J. Appl. Phys. 87 (2000) 7382.
[27] A.R. Armstrong, M. Holzapfel, P. Novak, C.S. Johnson, S.H. Kang, M.M. Thackeray, P.G. Bruce, J. Am. Chem. Soc. 128 (2006) 8694.
[28] C.R. Fell, D. Qian, K.J. Carroll, M. Chi, J.L. Jones, Y.S. Meng, Chem. Mater. 25 (2013) 1621.
[29] S. Hy, F. Felix, J. Rick, W.N. Su, B.J. Hwang, J. Am. Chem. Soc. 136 (2013) 999.
[30] Z. Lu, J.R. Dahn, J. Electrochem. Soc. 149 (2002) A815.